

Accepted for publication in Geophys. Astrophys. Fluid Dyn. 2004

Quasi-two-dimensional turbulence on the polar beta-plane: laboratory experiments

Y. D. Afanasyev^{*}, J. Wells

*Department of Physics and Physical Oceanography, Memorial University of
Newfoundland, St. John's, NL, Canada*

*Corresponding author:

Department of Physics and Physical Oceanography,

Memorial University of Newfoundland,

St. John's, NL, Canada A1B 3X7

e-mail: yakov@physics.mun.ca

fax: 1(709) 7378739

Abstract

Results from a new series of experiments on turbulent flows decaying in a thin layer of water with a free surface in a rotating circular container are presented. The flows are generated electromagnetically using a regular array of permanent magnets. The Particle Image Velocimetry method is used to determine the velocity and vorticity fields in the flow. The experimental results demonstrate the formation of a polar vortex and jets perturbed by stationary Rossby waves in experiments with higher values of the beta parameter. Blocking events similar to those occurring in the Earth's atmosphere were observed in the laboratory flows. The Two-dimensional energy spectra of the flow demonstrate anisotropy in the space of the azimuthal and total wavenumbers. The One-dimensional energy spectra are characterized by a peak at the Rhines wavenumber.

Keywords: beta-plane turbulence, zonal jets, Rossby waves

1. INTRODUCTION

Quasi-two-dimensional (Q2D) flows are a useful idealization in application to large scale motions of the atmosphere of the Earth and other planets as well as to the motion of the Earth's oceans. These flows have been a subject of study in a number of recent laboratory experiments with stratified and rotating fluids or the flows in a thin layer of fluid. In all of these cases different physical mechanisms suppress the motion in one direction and thus make the flow quasi-two-dimensional. A recent review of Q2D turbulence and in particular of turbulence on the beta-plane is given in Danilov, Gurarie (2000). When the Q2D turbulent flows occur on the beta-plane, the inverse energy cascade which is a characteristic of 2D turbulent flows in the absence of the beta-effect, is found to be arrested at a point which corresponds to the Rhines (1975) scale. Above this point the flow is predicted to be highly anisotropic with a dominant contribution of Rossby waves. It is due to the anisotropic dispersion relation of the Rossby waves that the distribution of energy in the wavenumber space becomes altered. Another (and related) effect of the variation of the Coriolis parameter with latitude on the turbulent flow is the redistribution of vortices of different sign in the North – South direction such that they form zonal jets. This results in a transfer of energy to the zonal component. The study of the emergence and persistence of these jets is clearly one of great interest since zonal jets have been observed in many geophysical systems and are a common feature in the atmospheres of Jupiter, Saturn and the Earth. A review of the different mechanisms of generation of geophysical jets is given by Rhines (1994).

A number of numerical studies have been performed in this area where the flow either on a Cartesian beta-plane or in the spherical geometry was simulated. A few important results relevant to the purpose of the present paper should be mentioned here. The evolution of the two-dimensional beta-plane energy spectrum obtained by Vallis and Maltrud (1993) demonstrated the formation of the dumbbell shaped region in the wavenumber space. This region is defined by the wave-turbulence transition as first predicted by Rhines (1975). A confirmation of the findings of Vallis and Maltrud was

provided for a spherical geometry by Nozawa, Yoden (1997) and Huang and Robinson (1998). The Formation of anticyclonic polar vortices was first reported by Yoden and Yamada (1993). Cho and Polvani (1996) who studied decaying turbulence on a sphere for a shallow water system showed that inside the polar vortex the potential vorticity (PV) is well homogenized and the polar vortex is bounded by large PV gradients. The formation of zonal jets (bands) is a typical feature of such simulations. The jet wavenumber measured in the simulations is usually close (Vallis and Maltrud, 1993) to the Rhines wavenumber predicted by theory. The formation of zonal jets is affected by bottom (linear) drag since the drag is important for the stabilization of the system (especially for the forced flow). Manfroi and Young (1998) found on the basis of a stability analysis of a barotropic zonal flow on the beta-plane that increasing the amount of bottom drag will directly effect both the final spacing and number of zonal jets. Danilov and Gurarie (2002) proposed a modification of the Rhines wavenumber that takes into account the bottom drag and confirmed its relevance to the jet wavenumber measured in their simulations of forced turbulence on the beta-plane. They also considered the friction wavenumber introduced by Lilly (1972), and concluded that organized jets appear when the Rhines wavenumber exceeds the friction wavenumber.

Flows on the beta-plane have been a subject of study in a number of laboratory experiments starting from the pioneering experiment by Whitehead (1975) where the flow on the polar beta-plane was induced locally by a vertically oscillating disc. The polar beta-plane was simulated by rotating a cylindrical container of water with a free surface such that the depth of the layer varies parabolically with radius. The result of this experiment was a narrow eastward (prograde) jet at the latitude of forcing and a broad westward flow outside of this region. Other ways to simulate the effect of varying Coriolis parameter with latitude are either to use a thin layer of uniform depth in a rapidly rotating container in a form of paraboloid (e.g. Nezlin and Snezhkin, 1993) or to modulate the depth of the layer using a container with a sloping bottom. Forcing for these experiments can then be provided in a number of ways. In some experiments a flow was induced by momentum and mass sources using a set of holes in the bottom of the tank. The fluid is pumped through one set of holes and simultaneously removed through another set. In the experiment by Colin de Verdiere (1979) a zonally traveling Rossby wave which was forced by a periodic excitation of sources and sinks located in a narrow zonal region close to the outer wall of the tank was shown to excite a mean flow. Using an array of sinks and sources located along a ring in the middle of the annulus, Aubret et al. (2002) were able to observe mixing of potential vorticity (PV) resulting in an occurrence of zonal flow pattern with regions specified by the location of the holes. Another type of forcing employs the classical method of differential heating of the annulus (Hide and Mason, 1975). A simple demonstrative experiment that can easily be reproduced using a phonograph turntable is described in Rhines (1994). The apparatus usually contains a cylindrical insert in the center. The inner walls are then cooled or the outer walls heated, or a combination of both. Cold water sinks at the inner wall while warm water rises at the outer wall resulting in radial flow towards the center of the container at the surface layer and in the opposite direction at the bottom. Radial motions are then converted into zonal flows by the Coriolis force. In experiments which follow this approach Bastin and Read (1998) were able to observe in such a baroclinic flow the formation of zonal jets as well as some stable eddy formations over a range of rotation

rates. Laboratory experiments provide an important alternative method of studying these flows. Different aspects of the dynamics of beta-plane turbulence including the process of PV mixing have been studied using experimental methods. However, a detailed investigation of the spectral characteristics of the flow is yet to be done. The major problem is to obtain the velocity field of the flow with a sufficiently high resolution. The main purpose of the present study is therefore to perform high resolution measurements of the velocity in the system with controlled forcing in order to demonstrate the occurrence of the dumbbell shaped two-dimensional spectra (lazy-8 in terminology by Holloway, 1984).

In the series of experiments reported herein, we choose electromagnetic forcing to generate the turbulent flow in a thin layer of conducting fluid. This method is widely used in investigations of two-dimensional turbulence (e.g. Marteau et al., 1995) and, we believe, has certain advantages as follows. This method allows us to create an approximately two-dimensional turbulent flow from the very start of the forcing. There are no baroclinic effects involved and the flow domain does not contain inner walls. Each magnet creates a horizontal vortex dipole (of zero total vorticity). This type of flows has been studied in detail (e.g. Voropayev and Afanasyev, 1992, 1994) and the characteristics of the dipole can be described in terms of the single control parameter, namely the dimensionless magnitude of the momentum flux (force) exerted by the magnet on the fluid. The length scale of the turbulent flow due to this forcing is simply determined by the spacing between the magnets (e.g. Wells and Afanasyev, 2004). In the following sections of this paper the characteristics of the flows generated by this method for different values of the rotation rate of the system are discussed. In this new sequence of experiments that document the evolution of the flow after the forcing was stopped the occurrence of zonal jets as well as Rossby waves and a laboratory representation of the polar vortex was observed. We then use the measured velocity fields to analyze quantitatively the integral characteristics of the flows as well as their spectral characteristics.

2. LABORATORY APPARATUS AND TECHNIQUE

The experiments were performed in a square tank of inner dimensions $L = 34$ cm and $W = 31.5$ cm (figure 1) which contained a circular insert of inner diameter $2R = 31$ cm. The container was filled with a single layer of salt water of height 1 cm and a concentration of 50 g/l. The flow was forced electromagnetically by imposing an electric current of magnitude 3A in the horizontal direction between two parallel electrodes located immediately outside of the circular insert. For this purpose, an array of 196 magnets were arranged with an equal spacing of 2 cm and alternating polarities immediately below a thin plastic sheet of thickness 0.02 cm that constituted the bottom of the container. Each magnet had a diameter of 1.4 cm and generated a magnetic field with a vertical component of approximately 0.09 T. The interaction of the magnetic field above each magnet and the electric current produced a localized horizontal force on the fluid in a direction perpendicular to both of these fields. Since the universal result of a localized force on a fluid is the generation of a vortex dipole, the combined result of the forcing in this case is initially an array of closely packed dipoles that share vortices with their neighbors. Due to the nonlinearity of the system, the vortices do not remain in a regular lattice, but instead they move creating a typical turbulent 2D field. In all of our

experiments the flow was initially forced for a period of time of 5-10 minutes and then was allowed to decay freely after the current was switched off.

In order to simulate in the laboratory the effect of the varying Coriolis parameter felt by an ocean or atmosphere on a rotating sphere we used a standard method where the depth of the rotating layer was varied with radial coordinates. The experimental tank was rotated at rates that varied from stationary to 3.1 rads/s in an anti-clockwise direction around a vertical axis through its center. Once solid body rotation was achieved, the surface of the water obtained a parabolic shape such that the depth, H , of the layer was

$$H = H_o + sr^2 \quad (1)$$

where $s = \Omega^2/2g$, Ω is the rotation rate of the platform, g is the gravitational constant, r is the radius and H_o is the height of the fluid at $r = 0$. The value for H_o was then calculated from the total volume of the fluid in the container and is given by

$$H_o = z_o - s \frac{(L^2 + W^2)}{12},$$

where z_o is the height of the fluid in the tank prior to rotation and L and W are the dimensions of the rectangular container. The experimental parameters are summarized in Table 1. In most of our experiments (1-21 in Table 1) z_o was chosen to be 1 cm. In experiments 22-26 (Table 1) the lower value of $z_o = 0.7$ cm was used. The same value of the depth of the fluid layer was used in our previous experiments with non-rotating two-dimensional turbulence (Wells and Afanasyev, 2004) and was shown to be large enough for the system not to be too dissipative. In experiments 22-26 (Table 1) the lower value of $z_o = 0.7$ cm was used to obtain a higher dissipation rate for comparison.

Instantaneous horizontal velocity fields of the flow were measured using Particle Imaging Velocimetry (PIV). Using this method, a video is taken of the flow and the motions of tracer particles are tracked between two successive images of this video. A more complete description of this method and general technique is given by Fincham and Spedding (1997) and Pawlak and Armi (1998). The tracer particles used in these experiments were small spheres of dyed wax with an average diameter of 1mm and a density slighter less than that of the salt water. The density of these beads was such that when added to the tank, they floated on top of the water and followed the flow. To produce a high contrast between the beads and the plastic bottom, the container was lit from above with two lamps.

Videos of the experiments were recorded in plan view using a digital video camera with an array resolution of 1032 x 1032 pixels. The typical spatial resolution of the images was 35.5 pixels/cm. The camera was fixed to the rotating platform to obtain images in the same frame of reference as the experimental tank and the videos were recorded directly into the memory buffers of a computer also situated on the rotating platform. Further processing of images was performed on workstations with double Alpha processors where successive images with a frame rate of 8.5 frames per second were used to obtain 4.25 velocity fields per second.

3. EXPERIMENTAL RESULTS AND INTERPRETATION

To characterize the regime of the flow and for the purpose of comparing it with the flows studied previously by other authors, it is useful to introduce the so-called γ and β -plane approximations. The potential vorticity (PV) is defined as:

$$q = \frac{\omega + f}{H}, \quad (2)$$

where ω is the relative vorticity, $f = 2\Omega$ is the planetary vorticity and H is the total height of the fluid at any given point in the tank. In a laboratory setting f is constant, while the total height H varies at different radii according to (1). Introducing a small parameter

$$\delta = \frac{sr^2}{H_0}$$

then allows us to write the potential vorticity as

$$q = \frac{(\omega + f)}{H(1 + \delta)} \approx \frac{(\omega + f)(1 - \delta)}{H_0}.$$

The assumption that the Rossby number $Ro = \omega / f \ll 1$, which is true for intermediate and later times during the flow evolution then gives

$$q = \frac{\omega + f \left(1 - \frac{sr^2}{H_0}\right)}{H_0}. \quad (3)$$

As a comparison, on a rotating sphere f varies with latitude as $f = 2\Omega \sin \alpha$. For small values of α (or equivalently for polar regions), we obtain

$$f = f_0 \left(1 - \frac{1}{2} \left(\frac{r}{R_E}\right)^2\right),$$

where r is the distance measured from the pole, $f_0 = 2\Omega$ and R_E is the radius of the sphere. This first order approximation to the actual variation of the Coriolis parameter near the

pole is known as the γ -plane approximation where $\gamma = \frac{f_0}{2R_E^2}$. The potential vorticity in

the polar region on the rotating sphere is then of similar form as the expression (3) for the laboratory system where the parameter γ can be introduced as $\gamma = \frac{fs}{H_0}$.

Next, we formally introduce the beta constant such that $f = f_0 + \beta y$ where y is measured from some intermediate radius r_0 . The potential vorticity (2) can be written as follows:

$$q = \frac{(\omega + f)}{H_0 + s(r_0 + y)^2} \approx \frac{\omega + f - \beta y}{H_0 + sr_0^2},$$

where

$$\beta = \frac{2sr_0}{H_0 + sr_0^2}. \quad (4)$$

The values of s , H_0 , and β are given in Table 1 for the different values of Ω used in our experiments. For these estimates the radius r_0 was chosen to be one half of the radius of the container.

To better understand the results of the laboratory experiments it is useful to perform a simple dimensional analysis of the control parameters involved in the problem. The flow can be characterized by the following set of dimensional parameters: the characteristic velocity, U , and the length scale, L , of the vortices, the depth, H , of the fluid layer, the kinematic viscosity, ν , the Coriolis parameter f and the parameter β . A set of four dimensionless parameters can then be obtained as follows:

$$\text{Ro} = \frac{U}{Lf}, \quad \text{E} = \frac{2\nu}{fH^2}, \quad \text{Re} = \frac{UL}{\nu}, \quad \beta^* = \frac{L^2}{U}\beta,$$

where Ro is the Rossby number, E is the Ekman number, Re is the Reynolds number and β^* is the dimensionless beta parameter. Taking typical values of the dimensional parameters to be $U = 0.5$ cm/s, $L = 4$ cm, $H = 0.5$ cm, $f = 3$ s⁻¹ and $\beta = 0.4$ cm⁻¹ s⁻¹ we can obtain the values of dimensionless parameters as follows

$$\text{Ro} \sim 4 \times 10^{-2}, \quad \text{E} \sim 3 \times 10^{-2}, \quad \text{Re} \sim 2 \times 10^2, \quad \beta^* \sim 1 \times 10^1.$$

Thus the Rossby number is small such that the flow is geostrophic to a significant degree. The Reynolds number is large enough for nonlinear effects to be significant. The value of β^* turns out to be comparable with characteristic values of this parameter for the atmospheric flows. Indeed, taking $U = 10$ m/s, $L = 6 \times 10^6$ m and $\beta = 4 \times 10^{-11}$ m⁻¹s⁻¹, we obtain the values of $\beta^* \sim 100 - 200$ for the Earth's atmosphere. In our high rotation experiments with $\beta = 1$ cm⁻¹ s⁻¹ when the scale of vortices (and zonal flows) becomes of order $L = 5 - 10$ cm, we obtain the values of the dimensionless beta in the same range. This indicates that our laboratory system can demonstrate the same dynamical phenomena as the Earth's atmosphere. The smallness of the Ekman number has important consequences for the effects of the dissipation of energy in the system. The

equation of conservation of potential vorticity in the form $\frac{Dq}{Dt} = 0$ implies inviscid flow.

The laboratory system, however, is dissipative. It is therefore important to characterize the dissipation quantitatively in order to be assured that it is not too restrictive. Bottom friction as well as friction due to ordinary viscosity causes the total energy of the flow to decay. Bottom friction is commonly parameterized by a linear term in the vorticity equation

$$\frac{D\omega}{Dt} = -\lambda\omega + \nu\Delta\omega,$$

where ω is vorticity, λ is the linear drag coefficient and ν is the kinematic viscosity. For a rotating system λ can be expressed as $\lambda = fE^{1/2}/2$. Equivalently, the characteristic Ekman time scale is $T_E = \lambda^{-1} = H/(\nu\Omega)^{1/2}$. The Ekman condition is valid for flows with low Rossby number. It works well however even for vortices with moderate Rossby number (e.g. Kloosterziel and van Heijst, 1992, Maas, 1993). Linear drag causes an exponential decay of energy. The values of the exponent of total energy decay $d(\ln E)/dt$ in our experiments are given in Table 1. This decay rate was measured during the intermediate time of approximately 5 s after the termination of the forcing. The values of the exponent compared with those ($d(\ln E)/dt = -0.024$ s⁻¹) obtained in our previous

experiments with nonrotating 2D turbulence (Wells and Afanasyev, 2004), turned out to be significantly larger. This can be explained by the fact that in the nonrotating experiments we used two-layer system, which shields the flow from the bottom. The exponent also increases (linearly) with the rotation rate Ω of the system. This is due to the fact that the average depth of the layer, which can be introduced as, follows:

$$D = \frac{1}{R} \int_0^R H(r) dr = H_0 + \frac{sR^2}{3} \quad (5)$$

decreases with rotation rate (see Table 1).

According to (Danilov et al., 2002) the mean exponent of energy decay due only to bottom friction can be estimated as

$$2\lambda = -\frac{d(\ln E)}{dt} - 2\nu \frac{Z}{E},$$

where E and Z are energy and enstrophy per unit mass. Here the contribution to the decay rate from the ordinary viscosity is given by the term $-2\nu Z/E$. In the above relation for λ this contribution is subtracted from the total rate of energy decay given by $d(\ln E)/dt$. In the nonrotating experiments the term $2\nu Z/E$ was responsible for approximately one half of the total dissipation rate. Since in the present experiments the value of this term was approximately the same as in the nonrotating case, but $d(\ln E)/dt$ was significantly larger, the bottom friction prevails. Neglecting the ordinary viscosity we obtain $2\lambda \approx d(\ln E)/dt$.

The series of 26 experiments discussed herein were performed for different values of the rotation rate of the system and therefore for different values of β . Typical pictures of the flow during the intermediate time of its evolution, shortly after the forcing was stopped are given in Figure 2 for two experiments with higher and lower values of β . There are clear differences between the two flows. The flow with higher β (Figure 2 a) is characterized by a well defined polar vortex with an intense prograde (cyclonic) jet at its periphery. The jet region is subject to wave-like perturbations of significant amplitude. This is clearly a typical Rossby wave which can also be considered as a vortex Rossby wave (Montgomery and Kallenbach, 1997, Montgomery and Lu, 1997) since it develops with significant background shear. The wave is almost stationary such that its phase moves only very slowly in the cyclonic direction as can be seen in an animated sequence of images of the flow. The graphs of zonally averaged potential vorticity (see Figure 3 a) demonstrate that potential vorticity in the flow with higher β is not mixed to any noticeable extent. The perturbations of the polar vortex are therefore “elastic” in accordance to theoretical results (e.g. Norton, 1994). The distribution of the zonally averaged azimuthal velocity (Figure 3 a) is characterized by a narrow prograde jet localized near $r = 8$ cm and a weak retrograde (anticyclonic) circulation in the center of the container (polar vortex). The space-time diagram (Hovmoller plot) in Figure 4 demonstrates the evolution of the zonally averaged flow. After the forcing stops the vortices in the turbulent flow redistribute themselves such that four (two prograde and two retrograde) jets develop. These jets eventually merge into a system that consists of a relatively strong prograde jet at the periphery and a weak retrograde circulation in the center of the domain. The potential vorticity map of the flow with lower β (Figure 2 b)

demonstrates a different regime of the flow in which the potential vorticity is mixed to a significant degree. This is also evident from the lower panel of Figure 3 b. The mixing is stronger in the center of the container where the gradient of the background vorticity f/H is weaker than that at larger radii. The vortices in the flow in Figure 2 b are round in contrast with the elongated vortices constituting “protuberances” at the periphery of the polar vortex in the flow in Figure 2 a.

Observations of the sequences of images that show the evolution of the flow with high and moderate values of β reveal another interesting phenomenon of geophysical relevance, namely the “blocking” of the jet. One of the clearest examples of this phenomenon that we observed is shown in Figure 5. The blocking occurred as a result of entrainment of a patch of lower PV between two protuberances. A vortex dipole with a direction opposite to that of the jet was formed and then remained stationary in the jet splitting it into two branches. The blocking lasted for approximately 2 rotations of the system (2 laboratory “days”). The relatively short period of blocking (in the Earth’s atmosphere blocking can last several days or even weeks) is most likely due to the fact that the flow itself is not stationary in our case. The distribution of PV along a line crossing the centers of the vortices in the dipole (Figure 6) shows a few interesting features of this structure. Outside of the dipole there is a strong gradient of PV, the jet surrounding the dipole is characterized by a uniform distribution of PV, while the protuberance in between the vortices of the dipole contains relatively high PV. The left hand vortex of the dipole contains relatively lower PV than in the right hand vortex as one might expect.

Further insight into the dynamics of the flow can be provided by an analysis of its spectral characteristics. The velocity components (v_x, v_y) were measured on a regular Cartesian grid of dimensions 99×99 . Since in our case it is natural to use the cylindrical polar coordinate system (r, θ), the velocity field was linearly interpolated onto a polar grid of dimensions 48×96 . The spacing between grid points in the radial direction was approximately the same as that in the Cartesian grid while in the azimuthal direction the data was undersampled at larger radii and oversampled near the center of the domain. The radial and azimuthal components (v_r, v_θ) of the velocity field were then estimated on the polar grid.

Each velocity component (v_r, v_θ), was decomposed using a Fourier transform in θ and Bessel function decomposition in r such that

$$v(r, \theta) = \sum_m \sum_n v_{mn} \exp(im\theta) J_n(\alpha_{mn} \frac{r}{R}). \quad (6)$$

The Bessel coefficients were obtained numerically by using the formula (Arfken and Weber, 2001)

$$v_{mn} = \frac{2}{R^2 [J_{n+1}(\alpha_{mn})]^2} \int_0^R v_m(r) J_n(\alpha_{mn} \frac{r}{R}) r dr \quad (7)$$

The two-dimensional power spectra $E_{mn} = v_{mn} v_{mn}^*$ in wavenumber space (n, m) were then calculated. Time averaging was performed over intervals of 1s. Note, that the one dimensional wavenumber $k = \alpha_{mn} / R$ can be introduced here. It is an analogy of the

radial wavenumber $k = (k_x^2 + k_y^2)^{1/2}$ defined for the two-dimensional Fourier transform in Cartesian coordinates. This follows from the comparison of the result of the application of the Laplacian operator on the basis functions

$$\varphi_{mn} = \exp(im\theta) J_m(\alpha_{mn} \frac{r}{R}) \text{ such that}$$

$$\nabla^2 \varphi_{mn} = -\alpha_{mn}^2 \varphi_{mn},$$

with the corresponding equation for the two-dimensional Fourier series (see e.g. Boer, 1983). The one dimensional energy spectrum $E(k)$ is obtained then by sorting the elements of the array E_{mn} according to the value of the corresponding wavenumber $k = \alpha_{mn} / R$. The zonal energy $E_z(k)$ is represented by the first line ($m = 0$) of the array E_{mn} . The typical two-dimensional energy spectra E_{mn} for two experiments with different rotation rates (and different β) are shown in Figure 7. The spectrum for the flow with lower value of β (Figure 7 b) is approximately isotropic which is indicated by the fact that it is aligned along the isolines of one-dimensional wavenumber k (white solid lines). The spectrum for the flow with higher β (Figure 7 a), on the other hand, is clearly anisotropic. This can be explained by the presence of Rossby waves in the flow. The dispersion relation for Rossby waves is anisotropic such that

$$\omega = \frac{\beta m}{r_0 k^2}. \quad (8)$$

Here ω is the wave frequency and r_0 is some intermediate radius which is introduced to estimate the dimensional azimuthal wavenumber m/r_0 . For our estimate we take $r_0 = R/2$. The turbulent frequency can be estimated as $\sigma = k V_{rms}$, where $V_{rms} = (2E)^{1/2}$ is the root mean square velocity. Taking the ratio of wave and turbulent frequencies

$$\frac{\omega}{\sigma} = \frac{2\beta m}{Rk^3 V_{rms}} \quad (9)$$

to be of order of unity, one obtains the anisotropic Rhines barrier (Rhines, 1975) between the wave dominated region of the spectrum and the turbulence dominated region. The dependence (9) is shown in Figure 7 in (m, n) space for three different values of the ratio ω/σ (white dashed lines). This is the analogue of the dumbbell shaped (lazy-8) two-dimensional spectrum in the polar coordinates. Rossby wave propagation must be a dominant phenomenon in the region within these curves (the interior of the dumbbell). The pattern of the spectrum in Figure 7 a is consistent in general with the isolines of ω/σ . The interior of the dumbbell contains less energy than its bounding surface as was expected from the theoretical and numerical analyses.

The typical evolution of the one-dimensional spectra of total energy for two experiments with different rotation rates are demonstrated in Figure 8. Solid lines in both plates in Figure 8 represent the spectra during the forcing period. Energy is distributed very evenly over the entire range of the wavenumbers for both of these flows and the spectra are very similar to one another. The spectra (circles in Figure 8) for the decaying flows after the forcing was stopped, however, reveal some differences. The most obvious difference is the position of the spectral peaks for these two flows. In the experiment (1 in

Table 1) with the higher rotation rate (and higher β) the peak is at higher wavenumbers than that for the experiment with lower rotation rate (15 in Table 1) as one might expect. A more subtle difference though is that while the spectral peak for the experiment with higher β does not change its position with time, the peak in the experiment with lower β shifts towards lower wavenumbers. This shift occurs in the same manner as that observed previously in our experiments with nonrotating two-dimensional turbulence (Wells, Afanasyev, 2004), namely the second (subharmonic) peak at $k_2 = k_1/2$ starts to grow while the peak at k_1 subsides. This corresponds to pairing of the vortex structures in the flow. This pairing is clearly restricted in the presence of the β -effect which rather induces zonal motions. One might also notice in Figure 8 that the slope of the graphs to the right (higher k) from the peaks is somewhat steeper (~ -5) in the higher rotation case. The value of the exponent is generally consistent with the results of numerical simulations (e.g. Yoden and Yamada, 1993). The high wave number part of the spectra is consistent with the power law of the form k^{-3} similar to that observed in our previous experiments with nonrotating two-dimensional turbulence. As one might expect the small scale vortices are unaffected by the system rotation.

It is useful to consider next the energy-weighted mean wavenumber k_E . It is introduced as

$$k_E(t) = \frac{M_1}{M_0}$$

where the n th moment M_n of the energy spectrum is (e.g. Scott, 2001)

$$M_n(t) = \int_0^{\infty} k^n E(k, t) dk .$$

The energy-weighted mean wavenumber provides a measure of the energy containing scale. A similar wavenumber k_{zonal} is also defined for the zonal energy spectrum. The above integral characteristics were estimated in our experiments by numerical integration of the appropriate moments of the one dimensional energy spectra. A typical evolution of k_E and k_{zonal} for the experiments is given in Figure 8. Both of the wavenumbers stay at some constant level during the forcing and then decrease rapidly to another constant value after the forcing was stopped. The mean values of k_E after the period of rapid decrease were measured for all of the experiments and presented in Figure 10 *versus* the Rhines wavenumber k_β . This wavenumber represents an isotropic barrier between waves and turbulence. It can be obtained from (9) by setting the ratio of frequencies to be unity and averaging over the values of the azimuthal wavenumber m . Neglecting the anisotropy by taking $m/R = k$, we then obtain

$$k_\beta = \left(\frac{\beta}{V_{rms}} \right)^{1/2} . \quad (10)$$

The graph in Figure 10 demonstrates that the values of the measured k_E are close to the theoretical estimate of k_β in the experiments with higher β . This result was not expected a priori because strictly speaking the estimate (10) implies to a steady flow rather than a decaying one. Values of k_E from a short series of experiments (22-26 in Table 1) where

the depth of the layer was 30% less than that in the rest of the experiments are denoted by different symbols in Figure 10. This series covers the same range of β but the energy decay rate in these flows is significantly higher. The points from this series however lie very close to the rest of the points which indicates that it is the β -effect rather than dissipation that provides the arrest mechanism at small wavenumbers. This fact demonstrates indirectly that dissipation is not a limiting factor in our experiments.

4. CONCLUSIONS

In summary, it can be concluded that a laboratory investigation of turbulence decaying in a thin layer of water with a free surface rotating in a circular container has revealed that a zonal flow in the form of strong prograde jets and a relatively weak retrograde circulation emerges from an initially chaotic flow. In the experiments with a relatively high value of the β parameter a polar vortex with “elastic” boundaries strongly perturbed by (stationary) Rossby waves, is a characteristic feature of the flow. In the experiments with a lower β potential vorticity in the center of the container is mixed to a significant degree and the evolution of the flow is similar to that of a Q2D turbulent flow without rotation. Vortex structures are subject to pairing interactions such that the integral scale doubles. Blocking events similar to those occurring in the Earth’s atmosphere were observed in the laboratory flows with high and medium β . The particular example of blocking demonstrated in Figure 5 is the laboratory analogue of the so-called “omega” block in the atmosphere – a high pressure (anticyclonic) region which has become displaced and is on the polarward side of the jet stream. It frequently occurs in the late winter and early spring in the Northern Hemisphere. The name comes from its resemblance to the Greek letter, Omega, when analyzed on upper air charts.

The two-dimensional energy spectra for the flow with low values of beta was found to be approximately isotropic since the spectrum lies along the isolines of the one-dimensional wavenumber k . The presence of Rossby waves is apparent however in the anisotropic spectrum for the flow with high values of beta. This spectrum is in general consistent with the isolines of the anisotropic Rhines barrier between the wave-dominated region of the spectrum and the turbulence dominated region.

Investigations of the one-dimensional energy spectra of the flow revealed that the position of the peak at short wavenumbers depends on the β parameter rather than on the dissipation rate of the flow. The inverse energy cascade is arrested at small wavenumbers in the experiments with relatively high values of the β parameter. The measured energy-weighted mean wavenumber is in agreement with the estimate provided by the isotropic Rhines wavenumber. The spectra are characterized by a steep (~ -5) slope to the right (higher k) of the energy peak. In the experiments with lower β the upscale energy transfer is not restricted and it occurs via growth of subharmonic peaks due to successive pairing of vortex structures.

Acknowledgements

The research reported in this paper has been supported by the Natural Sciences and Engineering Research Council of Canada under grants 228941-2000 and 227192-2000.

REFERENCES

- Arfken, G. B. and Weber, H. J., *Mathematical Methods for Physicists*, 5th edition, Harcourt/Academic Press, Burlington, 2001.
- Aubert, J., Jung, S. and Swinney, H. L., “Observations of zonal flow created by potential vorticity mixing in a rotating fluid”, *Geophysical Research Letters* **29**, 1876, doi:10.1029/2002GL015422 (2002).
- Bastin, M. E. and Read, P. L., “Experiments on the structure of baroclinic waves and zonal jets in an internally heated, rotating, cylinder of fluid”, *Phys. Fluids* **10**, 374 (1998).
- Boer, G. J., “Homogeneous and isotropic turbulence on the sphere”, *J. Atmos. Sci.*, **40**, 154 (1983).
- Cho, J. Y.-K. and Polvani, L. M., “The emergence of jets and vortices in freely evolving, shallow-water turbulence on a sphere”, *Phys. Fluids* **8**, 1531 (1996).
- Coline de Verdiere, A., “Mean flow generation by topographic Rossby waves” , *J. Fluid Mech.* **94**, 39-64 (1979).
- Danilov, S., Dolzhanskii, F. V., Dovzhenko, V. A. and Krymov, V. A., “Experiments on free decay of quasi-two-dimensional turbulent flows”, *Phys. Rev. E.* **65**, 036316-1 (2002).
- Danilov, S. D. and Gurarie, D., “Quasi-two-dimensional turbulence”, *Physics – Uspekhi.* **43**, 863 (2000).
- Danilov, S. and Gurarie, D., “Rhines scale and spectra of the β -plane turbulence with bottom drag”, *Phys. Rev. E.* **65**, 067301 (2002).
- Fincham, A. and Spedding, G., “Low cost, high resolution DPIV for measurement of turbulent fluid flow”, *Exps. Fluids* **23**, 449 (1997).
- Hide, R. and Mason, P. J., “Sloping convection in a rotating fluid”, *Adv. Phys.* **24**, 47 (1975).
- Holloway, G., “Contrary roles of planetary wave propagation in atmospheric predictability”, in G. Holloway and B. J. West, eds., *Predictability of Fluid Motions* (American Institute of Physics, New York, 1984), 593-599.
- Huang, H. P. and Robinson, W. A., “Two-dimensional turbulence and persistent zonal jets in a global barotropic model”, *J. Atmos. Sci.* **55**, 611 (1998).
- Kloosterziel, R. C. and van Heijst, G. J. F., “The evolution of stable barotropic vortices in a rotating free-surface fluid”, *J. Fluid Mech.* **239**, 607-629 (1992).
- Lilly, D. K., “Numerical simulation study of two-dimensional turbulence”, *Geophys. Astrophys. Fluid Dyn.* **3**, 289 (1972).
- Maas, L. R., “Nonlinear and free-surface effects on the spin-down of barotropic axisymmetric vortices”, *J. Fluid Mech.* **246**, 117-141 (1993).
- Manfroi, A. J. and Young, W. R., “Slow evolution of zonal jets on the beta plane”, *J. Atmos. Sci.* **56**, 784 (1998).
- Marteau, D., Cardoso, O. and Tabeling, P., “Equilibrium states of two-dimensional turbulence: An experimental study”, *Phys. Rev. E.* **51**, 5124 (1995).
- Montgomery, M. T. and Kallenbach, R. J., “A theory for vortex Rossby-waves and its application to spiral bands and intensity changes in hurricanes”, *Q. J. R. Meteorol. Soc.* **123**, 435 (1997).
- Montgomery, M. T. and Lu, C., “Free waves on barotropic vortices. Part I: Eigenmode structure”, *J. Atmos. Sci.* **54**, 1868 (1997).

- Nezlin, M.V. and Snezhkin, E. N., *Rossby Vortices, Spiral Structure, Solitons*, Springer-Verlag, Berlin, Heidelberg, 1993.
- Norton, W. A., “Breaking Rossby Waves in a Model Stratosphere Diagnosed by a Vortex-Following Coordinate System and a Technique for Advecting Material Contours”, *J. Atmos. Sci* **51**, 654 (1993).
- Nozawa, T. and Yoden, S., “Spectral anisotropy in forced two-dimensional turbulence on a rotating sphere”, *Phys. Fluids* **9**, 3834 (1997).
- Pawlak, G. and Armi, L., “Vortex dynamics in a spatially accelerating shear layer”, *J. Fluid Mech.* **376**, 1 (1998).
- Rhines, P. B., “Waves and turbulence on a beta-plane”, *J. Fluid Mech.* **69**, 417 (1975).
- Rhines, P. B., “Jets”, *Chaos* **4**, 313 (1994).
- Scott, R. B., “Evolution of energy and enstrophy containing scales in decaying, two-dimensional turbulence with friction”, *Phys. Fluids* **13**, 2739 (2001).
- Vallis, G. and Maltrud, M. E., “Generation of mean flows and jets on a beta plane and over topography”, *J. Phys. Oceanogr.* **23**, 1346 (1993).
- Voropayev, S. I. and Afanasyev, Y. D., “Two-dimensional vortex dipole interactions in a stratified fluid”, *J. Fluid Mech* **236**, 665 (1992).
- Voropayev, S. I. and Afanasyev, Y. D., *Vortex Structures in a Stratified Fluid*, Chapman and Hall, London, 1994.
- Wells, J. and Afanasyev, Ya. D., “Decaying quasi-two-dimensional turbulence in a rectangular container: laboratory experiments”, *Geophys. & Astrophys. Fluid Dyn.* **98**, 1 (2004).
- Whitehead, J. A., “Mean flow driven by circulation on a β -plane”, *Tellus* **27**, 634 (1975).
- Yoden, S. and Yamada, M., “A numerical experiment of two-dimensional decaying turbulence on a rotating sphere”, *J. Atmos. Sci.* **50**, 631 (1993).

Table 1.

Experiment Number	Ω (s ⁻¹)	$s = \Omega^2/2g$ (cm ⁻¹)	Ho (cm)	D (cm)	β (cm ⁻¹ s ⁻¹)	2λ (s ⁻¹)
1	3.1	0.0049	0.18	0.57	0.97	0.36
2	3.1	0.0049	0.18	0.57	0.97	0.33
3	3.1	0.0049	0.18	0.57	0.97	0.36
4	2.8	0.0041	0.32	0.64	0.63	0.32
5	2.8	0.0041	0.32	0.64	0.63	0.35
6	2.6	0.0034	0.44	0.70	0.41	0.30
7	2.6	0.0034	0.44	0.70	0.41	0.31
8	2.5	0.0033	0.45	0.71	0.40	0.39
9	2.3	0.0027	0.55	0.76	0.27	0.28
10	2.3	0.0027	0.55	0.76	0.27	0.27
11	2.0	0.0021	0.64	0.81	0.17	0.27
12	2.0	0.0021	0.64	0.81	0.17	0.29
13	1.8	0.0016	0.73	0.86	0.11	0.24
14	1.8	0.0016	0.73	0.86	0.11	0.25
15	1.5	0.0012	0.80	0.90	0.063	0.22
16	1.5	0.0012	0.80	0.90	0.063	0.22
17	1.3	8.1×10^{-4}	0.86	0.93	0.034	0.19
18	1.3	8.1×10^{-4}	0.86	0.93	0.034	0.20
19	1.0	5.1×10^{-4}	0.92	0.96	0.016	0.18
20	0.47	1.1×10^{-4}	0.98	0.99	0.0017	0.14
21	0.0	0.0	1.0	1.0	0.0	0.074
22	2.6	0.0034	0.14	0.40	0.78	0.50
23	2.0	0.0021	0.34	0.51	0.28	0.46
24	1.8	0.0016	0.43	0.56	0.17	0.44
25	1.5	0.0012	0.50	0.60	0.095	0.33
26	1.0	5.1×10^{-4}	0.62	0.66	0.024	0.30

Figure captions:

Figure 1. Sketch of the experimental setup. (a) top view (b) side view.

Figure 2. Vorticity (color) and velocity (arrows) fields measured in two experiments with high and low beta: experiment 5 (Table 1) at $t = 4$ s after the forcing was stopped (a) and experiment 15 at $t = 11$ s (b). The color bar shows the potential vorticity scale in $(\text{cm s})^{-1}$. The arrow in the top left hand corner of each frame represents the velocity scale, 1 cm/s. The total distance on the x and y axes is 31cm.

Figure 3. Radial distributions of azimuthally averaged zonal velocity and potential vorticity for two experiments with high and low beta: experiment 5 (Table 1) at $t = 4$ s after the forcing was stopped (a) and experiment 15 at $t = 11$ s (b). Solid lines represent distributions of planetary vorticity f/H .

Figure 4. Space-time diagram of the averaged zonal velocity for experiment 15. The grey scale represents velocity in cm/s.

Figure 5. Zoomed velocity and potential vorticity map for experiment 10 demonstrating the blocking event, $t = 8$ s after the forcing was stopped. The significant features of the flow are highlighted. The anticyclonic (A) and cyclonic (C) vortices that comprise the stationary dipole are marked as is a protuberance (P) at the periphery of the polar vortex. The solid line represents the line through the center of the dipole along which the distribution of PV was measured and the black arrow represents the direction of the zonal flow.

Figure 6. Distribution of potential vorticity along the straight line going through the centers of the vortices in the dipole in Fig. 3. The distribution is approximated by a piecewise linear dependence (solid line).

Figure 7. Two-dimensional energy spectra for two experiments with high and low beta: experiment 1 (Table 1) at $t = 4$ s after the forcing was stopped (a) and experiment 15 at $t = 11$ s (b). The grey scale represents $\ln(E_{mn})$. The vertical axis represents index m such that the first (top) line of the diagram shows the zonal spectrum. The solid white lines are isolines (from 0.5 to 5 with the interval 0.5 cm^{-1}) of the one-dimensional wavenumber $k = \alpha_{mn} / R$. The dashed white lines represent anisotropic wave-turbulence boundary in wave vector space given by (9). Contours corresponding to values of 0.5, 1 and 2 are shown.

Figure 8. Evolution of the one-dimensional energy spectrum for two experiments with high and low beta: experiment 1 (Table 1) (a) and experiment 15 (b). Solid lines represent the spectra during the forcing. Grey and black circles show spectra at $t = 2, 4$ s after the forcing was stopped (a) and $t = 1.5, 7$ s (b). Arrows indicate the position of the centroid of the total energy and zonal energy distributions.

Figure 9. Evolution of the energy-weighted mean scale k for the total energy (solid line) and for the zonal energy (dashed line) in the experiment 7.

Figure 10. Energy-weighted mean wavenumber k_E versus isotropic Rhines wavenumber k_β : circles - experiments 1- 21 (Table 1), stars - experiments 22- 26.

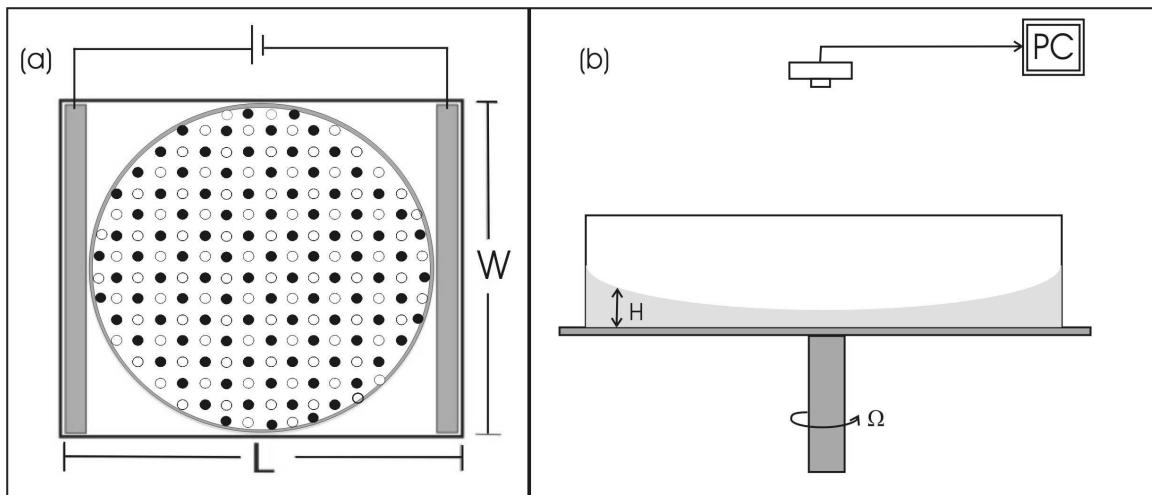


Figure 1

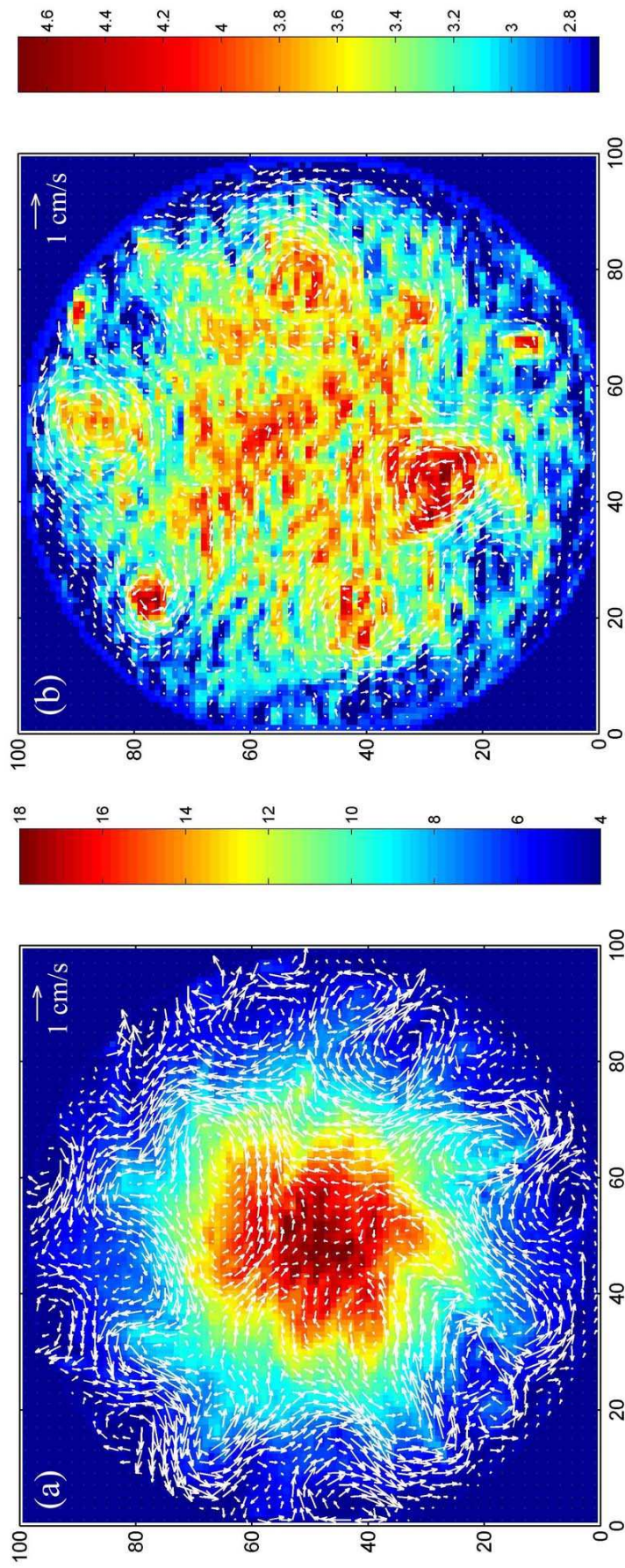


Figure 2.

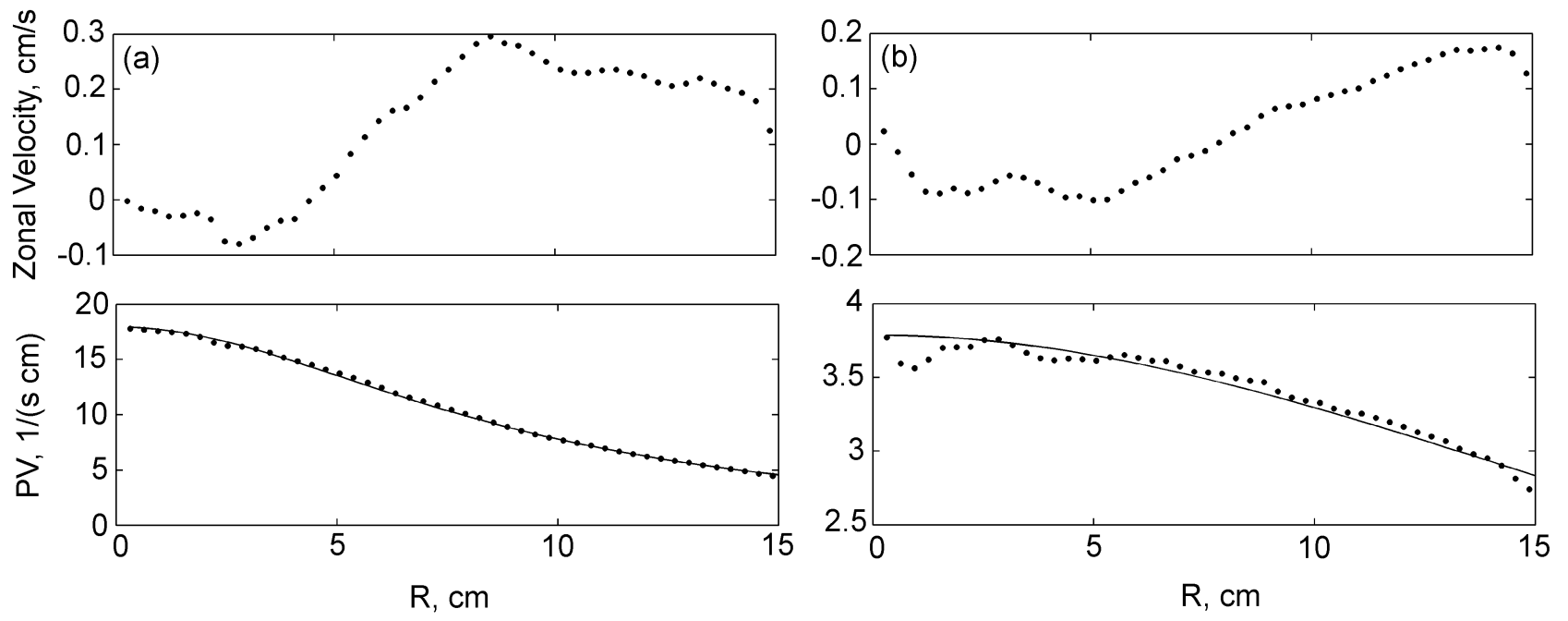


Figure 3.

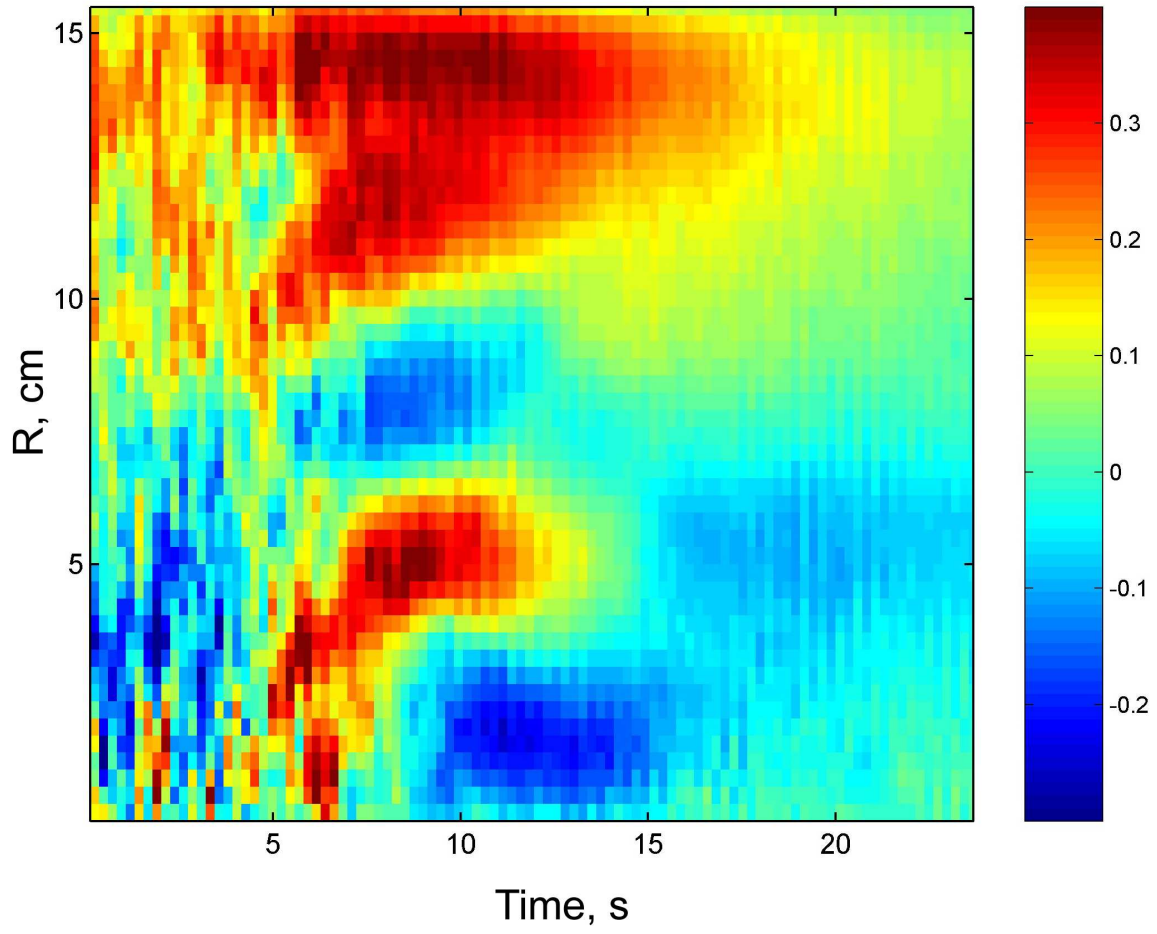


Figure 4

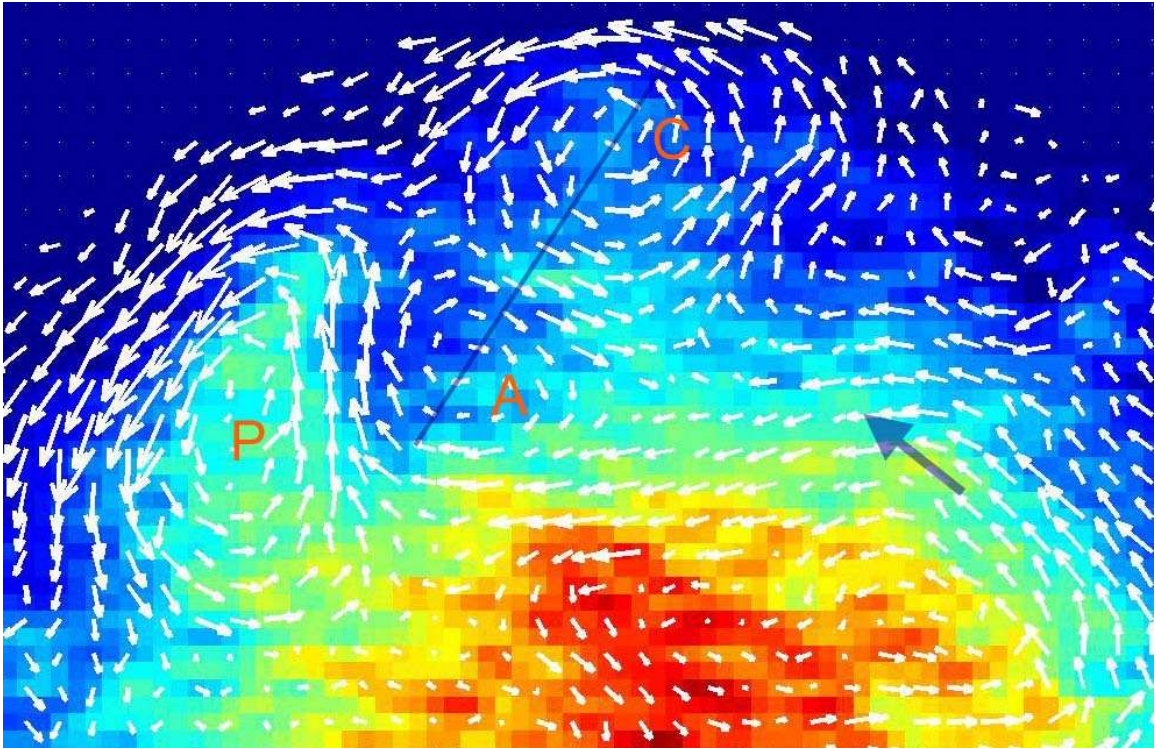


Figure 5

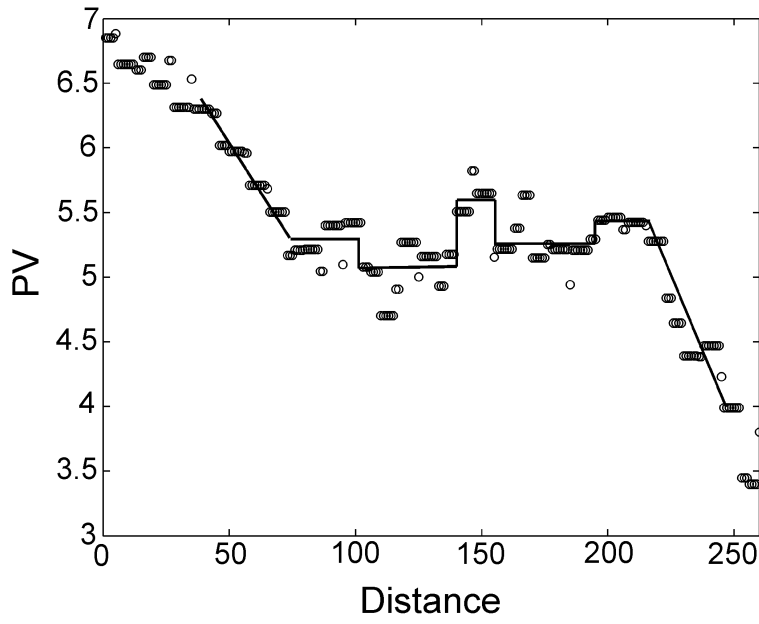


Figure 6

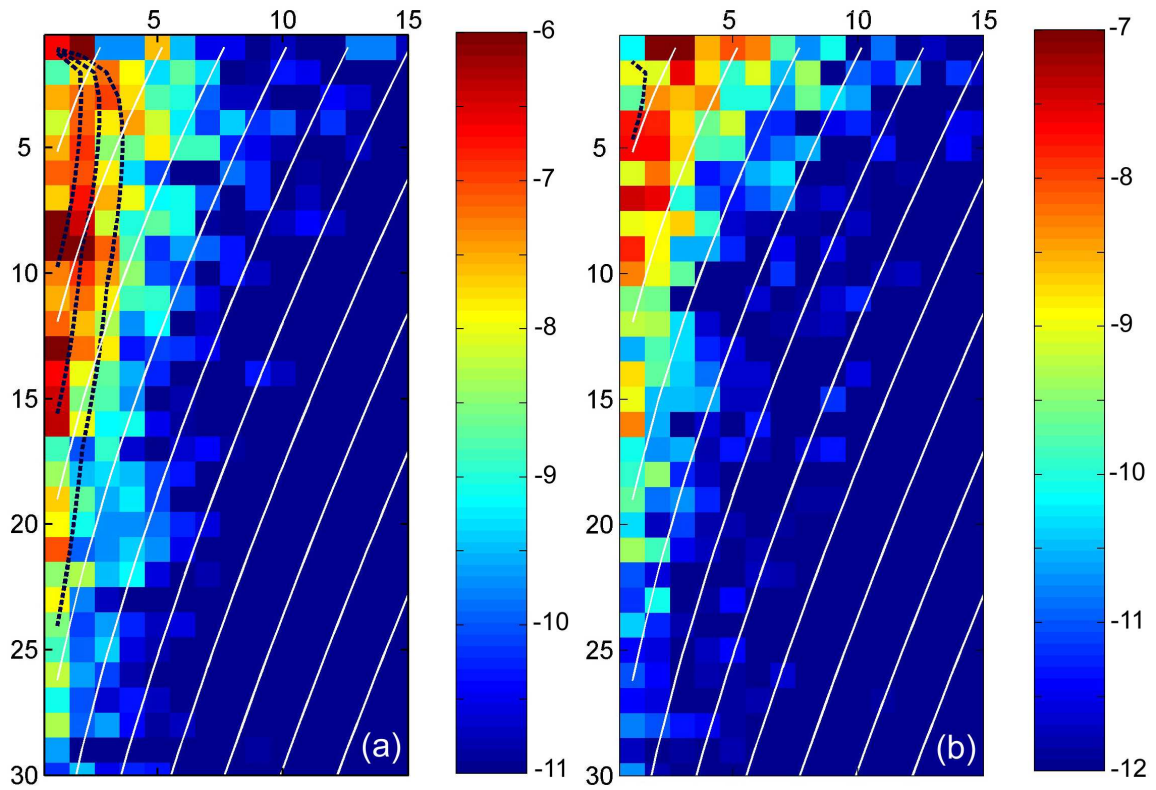


Figure 7

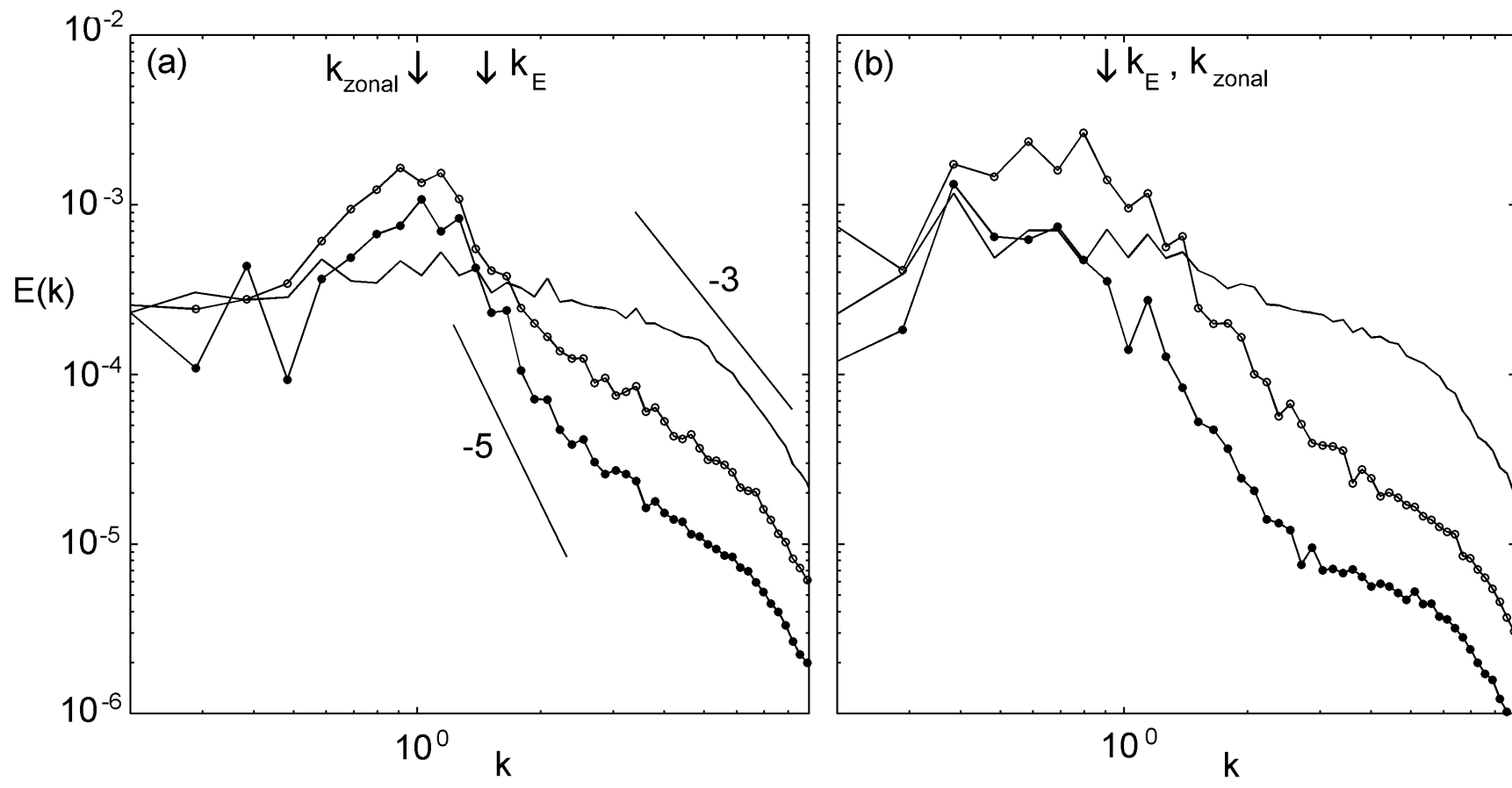


Figure 8.

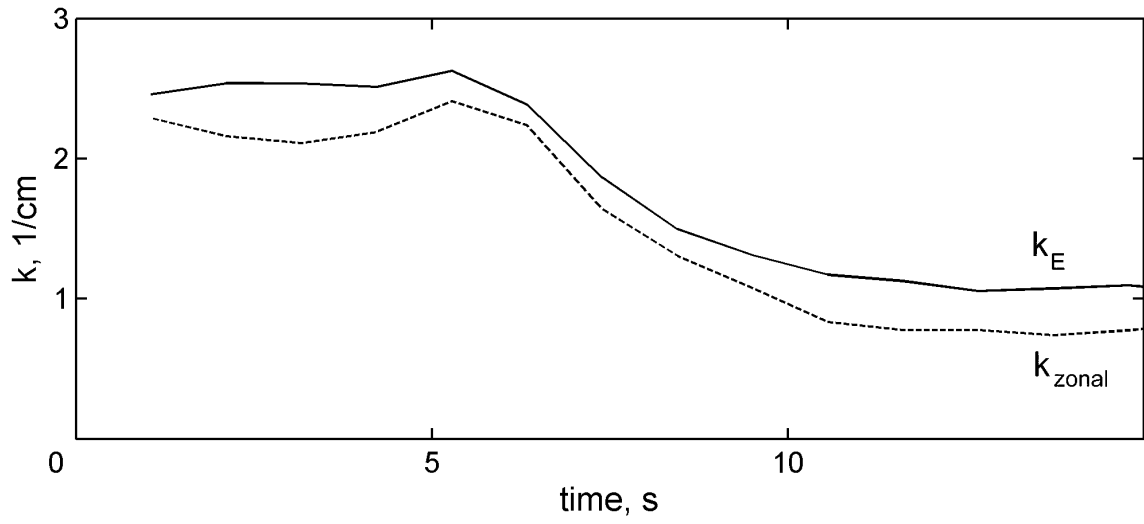


Figure 9

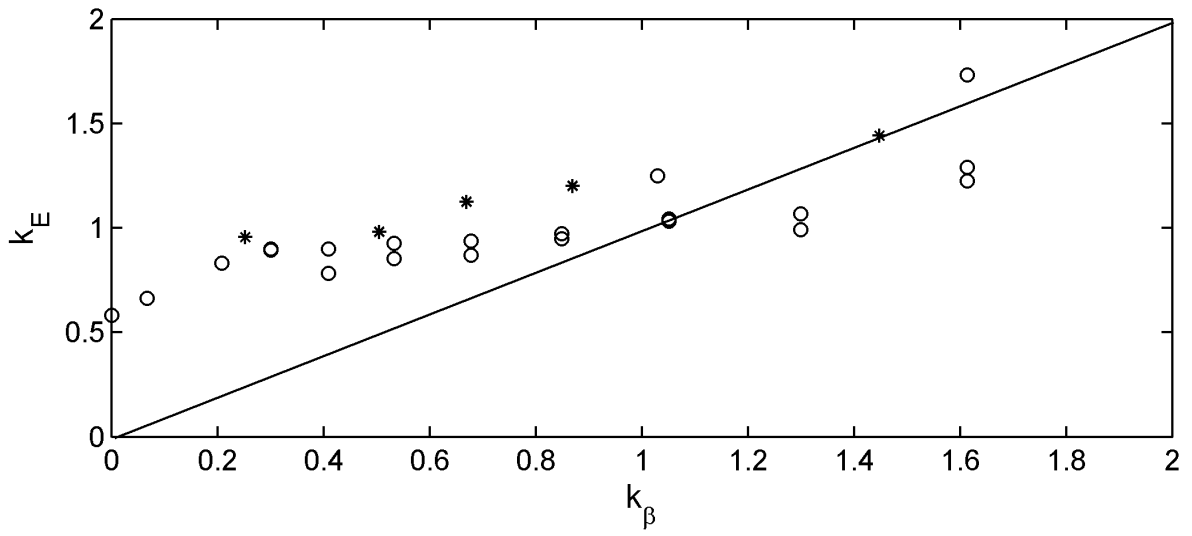


Figure 10